Scientific Research Publishing

Advances in Chemical Engineering and Science, 2025, 15(1), 17-30
https://www.scirp.org/journal/aces
ISSN Online: 2160-0406
ISSN Print: 2160-0392

Hydrogen Production from Glucose by Layered Double Oxides Photocatalysis

Moraya Alqahtani, Mohammed Bahattab, Mohammed Alabdulsalam, Issa Abaalkheel, Ahmad Almater

King Abdulaziz City for Science and Technology, Riyadh, Saudi Arabia
Email: mhalqhtani@kacst.gov.sa

How to cite this paper: Alqahtani, M., Bahattab, M., Alabdulsalam, M., Abaalkheel, I. and Almater, A. (2025) Hydrogen Production from Glucose by Layered Double Oxides Photocatalysis. *Advances in Chemical Engineering and Science*, **15**, 17-30.
https://doi.org/10.4236/aces.2025.151002

Received: September 30, 2024
Accepted: December 7, 2024
Published: December 10, 2024

Abstract

Hydrogen (H_2) production from renewable biomass resources plays a significant role in solving the shortage of fossil energy; hence, there is an interest in investigating alternative, cleaner processes. This work intends to study the photocatalytic production of hydrogen from D-(+)-Glucose by using different groups of catalysts that have been prepared (M^{2+} = Zn, Mg and Ni) M^{2+}/Ti^{4+} Al^{3+}-LDHs (layered double hydroxides). It is then loaded Pd on the catalyst, and the effect of the composite catalyst, layered double hydroxides, is measured. After calcining, the catalyst for the conversion of Layered Double Hydroxides (LDHs) to Layered Double Oxides (LDOs) is used to produce hydrogen gas from glucose. Photocatalytic reforming of glucose-derived compounds is an efficient method for the production of hydrogen. The purpose is to study the effect of metal ions on layered double oxide (LDO) materials by loading Pd and investigate hydrogen production from glucose. The metal cations in the layer were distributed through the preparation of the catalyst process by ion and atom scale between the layers, which were dispersed systematically, as well as the controlled component catalysis. This process shows that ZnTiAl-LDO had the best effect as a catalyst in producing hydrogen compared to NiTiAl-LDO and MgTiAl-LDO.

Keywords

Photocatalysis, Hydrogen Production, Layered Double Oxides (LDO), D-(+)-Glucose

1. Introduction

The increase in environmental concerns associated with the high demand for energy has been observed in the past decades. It is mostly due to population growth

and technological development. It has resulted in a great necessity to find alternative routes for obtaining clean energy from sources. The processes currently used to produce energy are mainly based on fossil resources that generate high levels of atmospheric pollution. This atmospheric contamination is related to the burning of hydrocarbons, which produces greenhouse gas emissions such as CH_4, CO_2, and NO_x. Due to these factors, a great effort has been put into trying to find economically and environmentally friendly routes to produce energy. Hydrogen is widely considered an attractive energy source for replacing conventional fossil fuels from both environmental and economic standpoints. Fujishima and Honda, in the 1970s, described a photocatalytic process to obtain hydrogen [1] [2]. The scientific community has devoted a huge interest in producing H_2 by photocatalytic processes.

Hydrogen is a promising source for obtaining energy because of its high energy and small dimension per unit mass, which is higher than fossil fuels. Another factor is the abundance on Earth. However, hydrogen exists on a large scale on Earth. This element is usually found in bond form, *i.e.*, linked to other elements such as water, and not as a sole molecule. This may constitute a disadvantage to others, such as safety, since hydrogen is lighter than air or has low ignition energy (0.02 mJ) when compared to fossil fuels (0.29 mJ for methane and 0.24 mJ for gasoline) [3]. On the other hand, when combined with fuel cell technology, it generates carbon-free energy and only water as a by-product. The production of hydrogen by glucose molecules can be considered an ideal route. This may be achieved by electrolysis or by photocatalytic water splitting. While the first process shows the disadvantage of requiring the use of high amounts of electrical energy, the second one has been considered a promising technology since H_2 production can be driven by solar light. However, the efficiency of this last process remains quite far from what is required for applicability. A common strategy usually applied to increase the efficiency of photocatalytic glucose is the addition of sacrificial reagents, usually alcohols, such as ethanol or methanol [4] [5]. Based on this principle, photocatalytic reforming processes gained importance since biomass-derived compounds such as saccharides, proteins, phenolic, etc.

It can be used as a sacrificial reagent for producing H_2. These compounds are usually industrial by-products with low commercial value and/or waste. Traditional methods of energetic valorization of such products are mostly based on thermal treatment at very high temperatures. Nonetheless, there is a great environmental disadvantage to this type of process for obtaining energy because the pyrolysis or organic matter originates from carbon-containing and other toxic gases that are the major ones responsible for atmospheric pollution. Photocatalysis is a catalysis field that deals with light-activated reactions. Heterogeneous photocatalysis is a physical-chemical process similar to typical heterogeneous catalysis but uses light instead of thermal activation and holds the following components: a reactant, a photon with adequate energy, and a semiconductor catalyst. Heterogeneous catalytic processes include the following steps: the transfer of the reactants

from the bulk to the catalyst surface, adsorption of the reactants followed by reaction on the catalyst surface, and desorption of the products. Photocatalytic processes only differ from these steps in the part of the reaction at the catalyst surface. This happens after the absorption of the photons by the semiconductor catalyst, followed by the creation of electron-hole pairs, which dissociate and form photoelectrons and positive holes (electron vacancies). After that, surface reactions happen, such as ion sorption, charge neutralization, radical formation, etc. [6] [7]. LDHs have been intensively studied recently as photocatalysts are supported because of the special structure and composition of the LDHs, which can be directly prepared or heat-treated. Layered double hydroxides are groups of anionic materials from clays that naturally occur from materials composed primarily of mulct-grained minerals. LDHs are based on positively charged brucite-like sheets, and the intercalation of anions balances the positive charges in the hydrated interlayer regions [8].

The LDH materials have the following general formula:

where e.g., $[M^{2+}]$—as contain of divalent cation (Zn^{2+}, Mg^{2+}, Cu^{2+}, Fe^{2+}, Ni^{2+}, Co^{2+}, Cu^{2+}, etc.). $[M^{3+}]$—as contain of trivalent cation (Fe^{3+}, Al^{3+}, Cr^{3+}, Ce^{3+}, Ti^{4+}, Zr^{4+}, etc.). $[A^{n-}]$—is a non-framework charge compensating exchangeable anion of charge n (CO_3^{2-}, NO_3^-, Cl^-, SO_4^{2-}, etc.) [14]. Where Containing M(II) and M(III), which exemplify divalent and a trivalent metal ion, shows the importance of the work on clays and the power composition configured. LDHs have special properties such as (I) a relatively simple synthesis procedure by inexpensive precursors, (II) adjustable layers element of structure, and (III) high thermal stability and high specificity [9].

Layered double hydroxides (LDHs) are Hydrotalcite-like compounds (HTlc) that have attracted substantial attention from both industry and academic research. Based on the above idea, we synthesized three kinds of layered double hydroxides in this paper: M^{2+}/TiAl-Pd-LDO (M = Mg, Ni, and Zn). The photochemical performance of hydrogen production from glucose by these LDH materials under visible light and the effect of metal ions on the photochemical performance were studied [10] [11]. Glucose is a common bioresource and product of photosynthesis, and it is renewable, non-toxic, inexpensive, and carbon-neutral throughout its entire life cycle. Glucose has the generality of a versatile renewable resource that can be utilized for the sustainable production of hydrogen [12] [13].

2. Experimental

2.1. Materials

All the reagents were analytical grade (AR) and used without further purification. They were purchased from Sigma-Aldrich Corp and Beijing Chemical Reagents Co. Deionized water was decarbonized by boiling and bubbling N_2 before employ-

ing all synthesis steps.

2.2. LDHs Layered Double Hydroxides Catalysts Synthesis of (M^{2+} = Zn, Mg and Ni) $M^{2+}/Ti^{4+}Al^{3+}$-LDHs Layered Double Hydroxides

Layered double hydroxides were synthesized by a co-precipitation method. The synthetic method was described as follows: an aqueous, (A) solution (200 mL) containing 3.60 g, NaOH (0.09 mol) and (B) solution (200 mL) containing 9.55 g $Zn(NO_3)_2{\cdot}6H_2O$ (0.032 mol) or 8.205 g $Mg(NO_3)_2{\cdot}6H_2O$ (0.032 mol) or 9.305 g, $Ni(NO_3)_2{\cdot}3H_2O$ (0.032 mol) of salts. Then, both solutions were added dropwise together into Na_2CO_3 (100 mL) in a flask with vigorous stirring until the final pH of (7) ± 0.2. Then, the heat of the reaction was raised to 65˚C for 18 h and then washed with hot deionized water three times to bring the pH down to 7. Finally, it was dried in an oven at 65˚C for 18 h, then ground, giving the product M^{2+}/Ti^{4+} Al^{3+}-CO_3-LDHs.

2.3. Characterization

Thermogravimetric Analysis (TGA) from Nietzsche (STA 449F3) was used, which was equipped with a crucible volume = 0.05 mg with a lid. The sample was heated from 20˚C to 700˚C with 5/min in a streaming nitrogen. Powder X-ray diffraction (XRD) patterns were registered on a Riga ku RINT 2000 powder diffractometer, using (λ = 1.54Å) at 40 kV and 178 mA and a scanning rate of 10˚/min in the range of 3˚ - 70˚. (UV) The transitions that result in the absorption of electromagnetic radiation and, also, where the ultraviolet (UV) for the region scanned is normally from 200 to 900 nm of the spectrum are transitions between electronic energy levels means for a Shimadzu UV-3600 spectrometer equipped for an integrating sphere attachment using $BaSO_4$ as background. Brunauer Emmett-Teller (BET) specific surface area analysis determines the specific surface area (m^2/g) of samples or, as a means of determining material by BET, the specific surface area for a sample measured to include the pore size distribution into the sample. The scanning electron microscope (SEM) uses a focused beam for high-energy electrons to produce a variety of signals on the surface of solid specimens to be analyzed. (Using EDS) It is capable of performing analyses of selected point locations in the samples; this tactic is especially useful in semi-quantitatively or qualitatively determining chemical composition elements that can be scanned at specific points. Transmission Electron Microscopy (TEM) is a technique from type a microscopy whereby a beam of electrons is transmitted through an ultrathin sample. An image is formed by the interaction of the electrons transmitted through the specimen.

3. Results and Discussion

3.1. Thermogravimetric Analysis (TGA)

Figure 1 shows the TGA of ZnTiAl-Pd-LDHs, MgTiAl-Pd-LDHs, and NiTiAl-

Pd-LDHs to convert the catalysts from to ZnTiAl-Pd-LDOs, MgTiAl-Pd-LDOs and NiTiAl-Pd-LDOs that used as reference and heated from 25˚C to 700˚C with rate 5/min in air. There are the measurements and the gradient for samples were started at 20˚C temperature. All catalysts put in a crucible where the calcination process stabilized the samples disintegrated at 400˚C for 4 hours [10]. After calcination, the removal of water interlayer physically adsorbed on the external surface of the crystallites and removal of interlayer anions, with a weight loss rapidly of the catalyst. Where LDOs are destroyed and these obvious peaks disappear, reflection forms an amorphous material after calcination [14] [15].

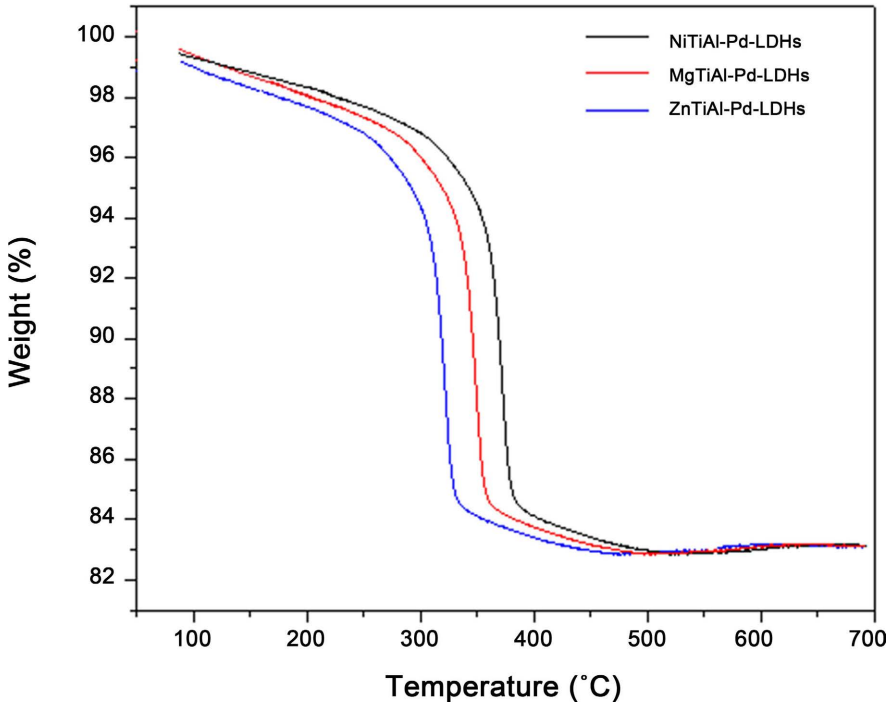

Figure 1. TGA of calcining ZnTiAl-Pd-LDHs, MgTiAl-Pd-LDHs and NiTiAl-Pd-LDHs.

3.2. XRD of (M^{2+} = Zn, Mg and Ni) $M^{2+}/Ti^{4+}Al^{3+}$-CO_3-LDHs

Figure 2 shows all crystal structures of the pristine ZnTiAl-LDHs, MgTiAl-LDHs, and NiTiAl-LDHs. Samples were examined by XRD for studying structure information and morphology of the Ti-containing LDHs (1) ZnTiAl-LDHs, (2) MgTiAl-LDHs, and (3) NiTiAl-LDHs. They were successfully prepared by using the co-precipitation method. **Figure 2** shows XRD patterns diffraction patterns of (1) ZnTiAl-LDHs, (2) MgTiAl-LDHs, and (3) NiTiAl-LDHs. It can be seen from **Figure 2** that the reflection diffraction peaks of two Theta degrees at (11.9˚, 23.6˚, 34.8˚, 46.8˚, 60.3˚, 61.7˚) correspond to the characteristic diffraction facets of (003), (006), (009), (015), (018), (110) and (113), respectively, of LDHs. It was found that the basic reflection (2 ≈ 11.9˚, d^{003} = 0.788 nm) for (1) ZnTiAl-LDHs. (2) MgTiAl-LDH shows similar reflections with a basal spacing (2 ≈ 11.9˚, d^{003} = 0.774 nm), which is indicative of different interlayer anions. In addition, it has been found that the basic reflection (2 ≈ 11.9˚, d^{003} = 0.722 nm) for (3) NiTiAl-

LDHs. The Bragg reflections sharp is well defined for ZnTiAl-LDHs, which appear sharper and show more complete peaks. It has a much better crystallinity compared with NiTiAl-LDHs and MgTiAl-LDHs. The presence of one reflection peaks in the sample with the highest $Ti^{4+}Al^{3+}$contents, which can be due to the intercalation of NO_3 ions coexisting with intercalated CO_3^{2-} ions. All catalysis diffraction peaks can be indexed by a rhombohedral structure with refined lattice parameters, which are steady with those of well-known LDH materials in CO_3^{2-} sharp form. This variation in the cell parameter could be due to the different $M^{II}/Ti^{4+}Al^{3+}$ ratios in the materials since the increase in the positive charge could produce a higher repulsion between the material layers. LDHs can interchange the intercalated anions with different kinds of anionic molecules [16] [17]. The small incongruity is due to the estimation error of the water content and the residual carbonate ions in the reaction [18]. These values were similar to those reported in the literature [19].

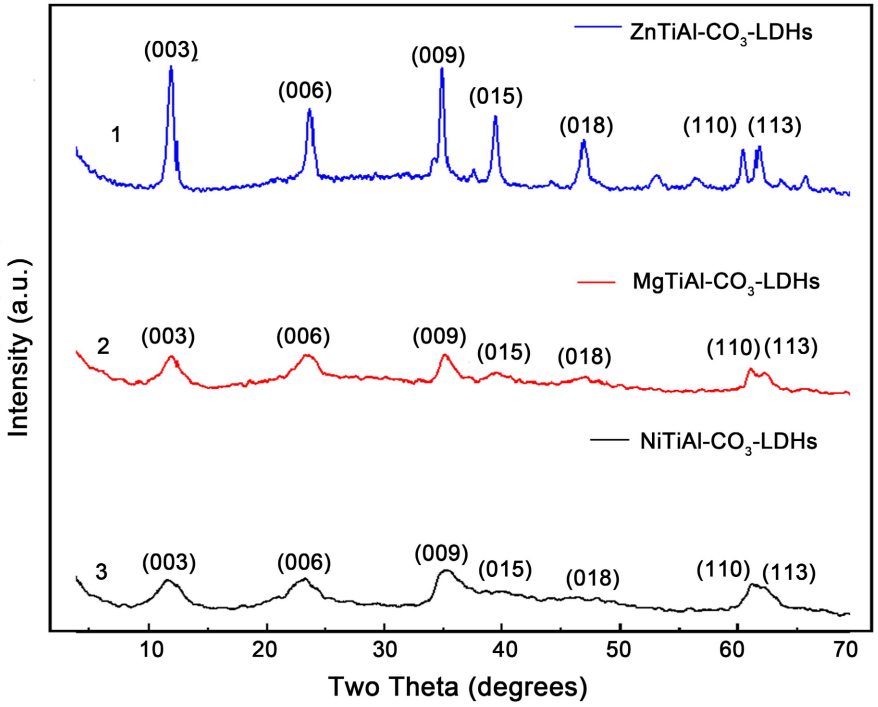

Figure 2. XRD patterns of (1) ZnTiAl-CO_3-LDHs, (2) MgTiAl-CO_3-LDHs, and (3) NiTiAl-CO_3-LDHs.

3.3. N_2 Adsorption-Desorption Isotherms and Surface Area of (M^{2+} = Zn, Mg and Ni) $M^{2+}/Ti^{4+}Al^{3+}$-CO_3-LDO

Samples were analyzed using the N_2-sorption isotherm, BET surface area, and Band Energy values for all the samples, which are shown in **Figure 3** and **Table 1**, where there are obvious differences in surface area for the three catalysts. The N_2 adsorption-desorption isotherm at 77 K and the corresponding pore size distribution curves for (A) ZnTiAl-Pd-LDO, (B) NiTiAl-Pd-LDO, and (C) MgTiAl-Pd-LDO are shown in **Figure 3**. H3-type hysteresis loop (P/P0 > 0.4) suggests the

presence of mesoporous for all catalysts. The better catalyst (A), ZnTiAl-Pd-LDO, shows the largest surface area (204.2645 m^2/g) and band gap (2.86 eV), the highest availability activity for UV radiation among them as compared with other catalysts. Catalyst (B) NiTiAl-Pd-LDO surface area (175.5964 m^2/g) and band gap (3.02 eV). Catalyst (C) MgTiAl-Pd-LDO surface area (116.3723 m^2/g) and band gap (3.30 eV). This difference in the surface area of the catalyst is due to the change of the metal catalyst [9].

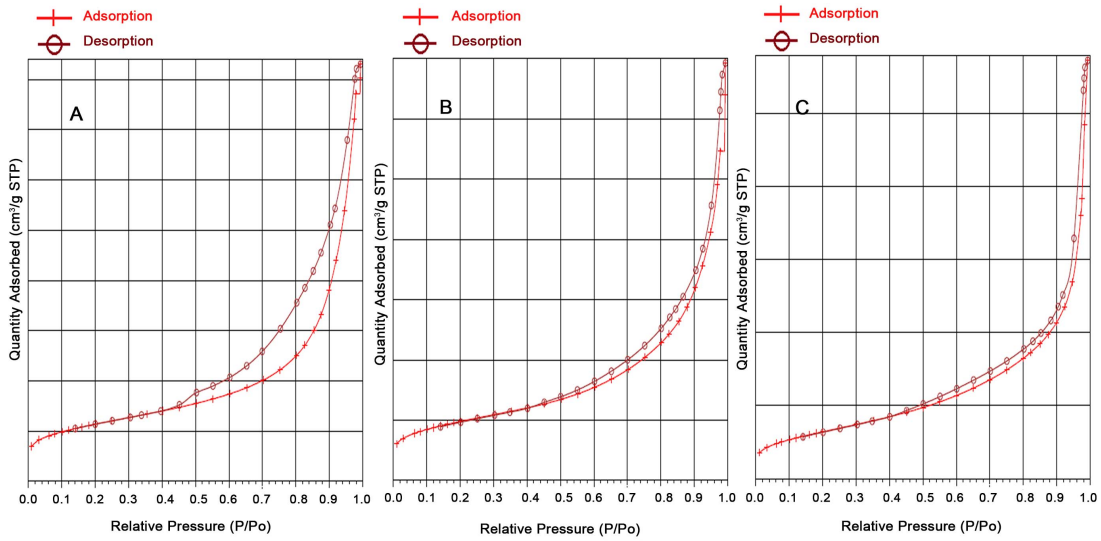

Figure 3. N_2 sorption isotherms of pore volume for (A) ZnTiAl-Pd-LDO, (B) MgTiAl-Pd-LDO, and (C) NiTiAl-Pd-LDO.

Table 1. BET specific areas of (M^{2+} = Zn, Mg, and Ni) M^{2+}/Ti^{4+} Al^{3+}-CO_3-LDO.

Catalyst	BET Surface Area $m^2 \cdot g^{-1}$	Band gap (eV)
ZnTiAl-Pd-LDO	204.2645 m^2/g	2.86 eV
NiTiAl-Pd-LDO	175.5964 m^2/g	3.02 eV
MgTiAl-Pd-LDO	116.3723 m^2/g	3.30 eV

3.4. UV-Vis Curves of (M^{2+} = Zn, Mg and Ni) $M^{2+}/Ti^{4+}Al^{3+}$-CO_3-LDO

Figure 4(A) for all catalysts for (M^{2+} = Zn, Mg, and Ni) $M^{2+}/Ti^{4+}Al^{3+}$-CO^3-LDO, LDO presented enhanced high absorption in the UV region (200 - 400 nm). The light absorption of the material and the transmigration of the light-induced electrons and holes are the keys to observing the photocatalytic reaction. The strong adsorption energy toward the molecules enhances the generation of photoinduced electro-hole pairs in active positions. Its comparison of the congruent absorption spectra between catalysts is clear. The results showed that UV-vis absorption of ZnTiAl-Pd-LDO followed the order of NiTiAl-d-LDO and MgTiAl-Pd-LDO. It can also inhibit the recombination and arrangement between photoelectrons and holes, but it is also an effective way to facilitate the rapid transfer of photoelectrons from bulk to the surface of catalysts.

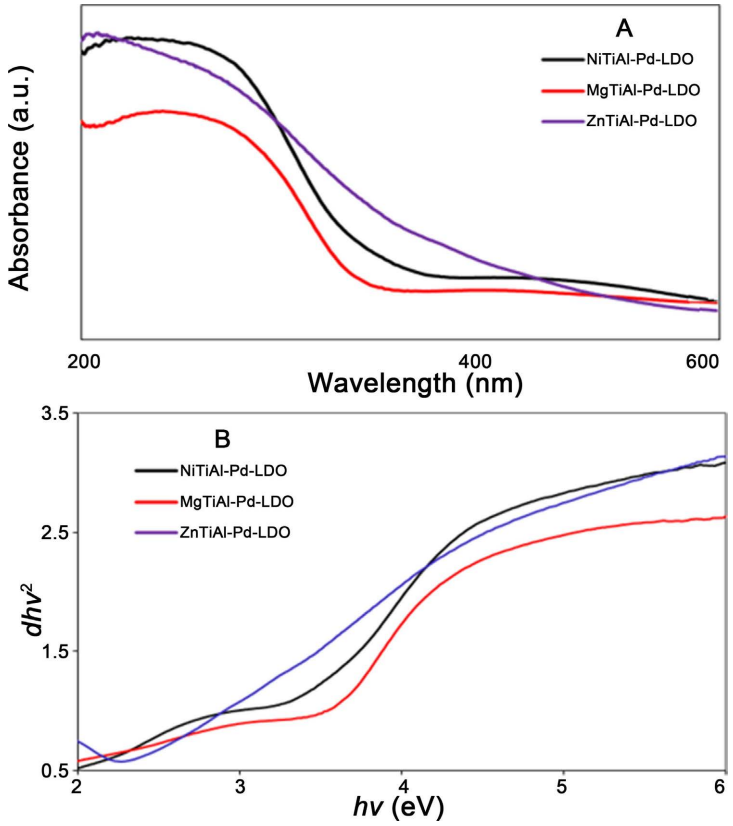

Figure 4. The UV-vis curves of (1) ZnTiAl-Pd-LDO, (2) MgTiAl-Pd-LDO, and (3) NiTiAl-d-LDO.

Figure 4(B) shows the UV-vis absorption spectra reflectance in diffuse for (M^{2+} = Zn, Mg and Ni) M^{2+}/Ti^{4+} Al^{3+}-CO_3-LDO, where the band gap was calculated by using the formula (Eg) = 1240/λ (nm) consecrated. The wavelength was calculated using an approximate value conforming to the slope of the straightest line near the edge of the absorption onset. This is signifying proof of the directly allowed optical transition. We could view the band gap (Eg) of the catalysts. **Table 1** shows the values of the difference between the band gaps in the catalysts. The results showed that the calculated band gap of ZnTiAl-Pd-LDO followed the order of ZnTiAl-Pd-LDO (2.86 eV) NiTiAl-d-LDO (3.02 eV) MgTiAl-Pd-LDO (3.30 eV) [9] [20] [21].

3.5. SEM Images of (M^{2+} = Zn, Mg and Ni) $M^{2+}/Ti^{4+}Al^{3+}$-CO_3-LDO

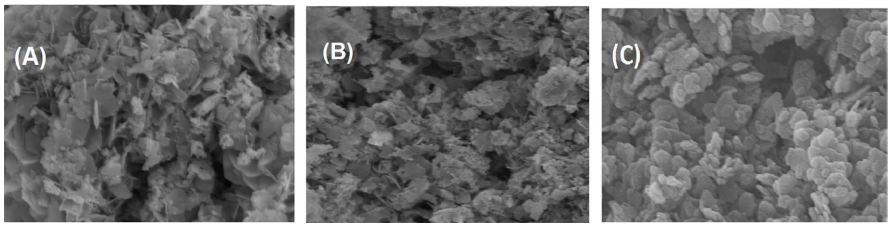

Figure 5. SEM Images of (A) ZnTiAl Pd-LDO, (B) NiTiAl-Pd-LDO, and (C)MgTiAl Pd-LDO.

Figure 5 shows the LDO of all samples that were analyzed by scanning electron microscope (SEM). The synthesized nanocomposite has been dispersed in ethanol for 10 min with mixed. Then, take a drop of the attached from a sample of the compound of the catalyst and place it on the carbon area in coated Cu. The SEM technique has been utilized to study the morphology of the nanoparticles, as can be seen in Figure 5. Scanning electronic microscope (SEM) in images of (A) ZnTiAl-LDO, (B) NiTiAl-LDO, and (C) MgTiAl-LDO shows the main elements in the rhombohedral symmetry.

The synthesized Figure 5(A) and Figure 5(B) are composed of numerous nanoflakes and revealed very small irregular flakes and plate-like structures of different sizes. The Pd-LDH materials show particle sizes in the range of 100 nm. In addition, Figure 5(C) shows a nanosheet with interlocking hexagonal shapes that has a more pronounced topography [22] [23].

3.6. EDS of (M^{2+} = Zn, Mg and Ni) $M^{2+}/Ti^{4+}Al^{3+}$-LDO

Figure 6 and Table 2 show the confirmation of the chemical composition of the crystal product by SEM-EDS analysis. Where the main elements analysis results show the chemical composition of the crystals by the molar ratio of the elements that had been prepared in (A) NiTiAl-CO_3-Pd-LDO (B) ZnTiAl-CO_3-Pd-LDO and (C) MgTiAl-CO_3-Pd-LDO. This is to prove that the Pd was loaded on the surface of the catalyst LDHs. The EDS results roughly proved the composition of synthetic LDO, although the values cannot represent the accurate percent of each element from area [22] [23].

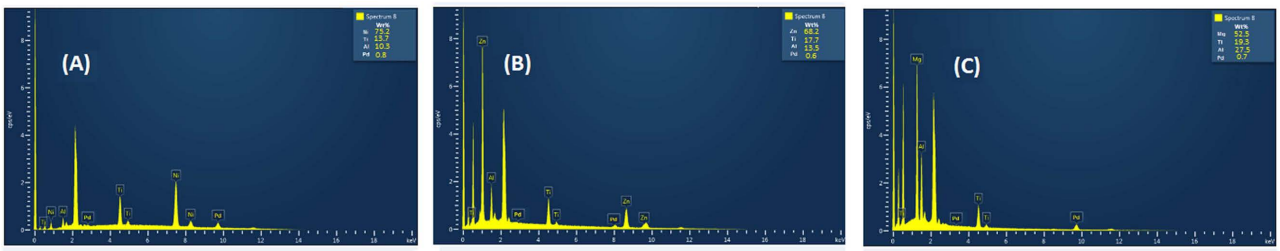

Figure 6. EDS Images of (A) NiTiAl-Pd-LDO, (B) ZnTiAl-Pd-LDO, and (C) MgTiAl-Pd-LDO.

Table 2. EDS of (A) NiTiAl-Pd-LDO, (B) ZnTiAl-Pd-LDO, and (C) MgTiAl-Pd-LDO.

Catalysis	Ni%	Zn%	Mg%	Ti%	Al%	Pd%	Total%
NiTiAl-Pd-LDO	75.2	-	-	13.7	10.3	0.8	100%
ZnTiAl-Pd-LDO	-	68.2	-	17.7	13.5	0.6	100%
MgTiAl-Pd-LDO	-	-	52.5	19.3	27.5	0.7	100%

3.7. TEM Images of ZnTiAl-Pd-LDO

Figure 7 shows the TEM images of the ZnTiAl-Pd-LDO nanocomposite. The synthesized nanocomposite was dispersed in ethanol for 10 minutes after mixing. Then, take a drop of the attached from a sample of the compound of the catalyst

and place it on the carbon area in coated Cu. It is revealed that the thickness of the hexagonal plate-like structure is only about 50 nm. Figure 7 shows representative TEM images of LDO after photo-loading of Pd 1 wt% by UV irradiation times 120 min and after calcination at a temperature of 400˚C. It can be observed that LDO is the formation of a sheet-like structure with a particle size of 50 nm. This confirms the agglomeration of Pd particles on the surface of the LDO by transmission electron microscopy Figure 7. Palladium nanoparticles appear as dark spherical spots in these samples. Pd nanoparticles are heterogeneously distributed on the LDO surface area, and particle sizes higher than 50 nm were observed [24].

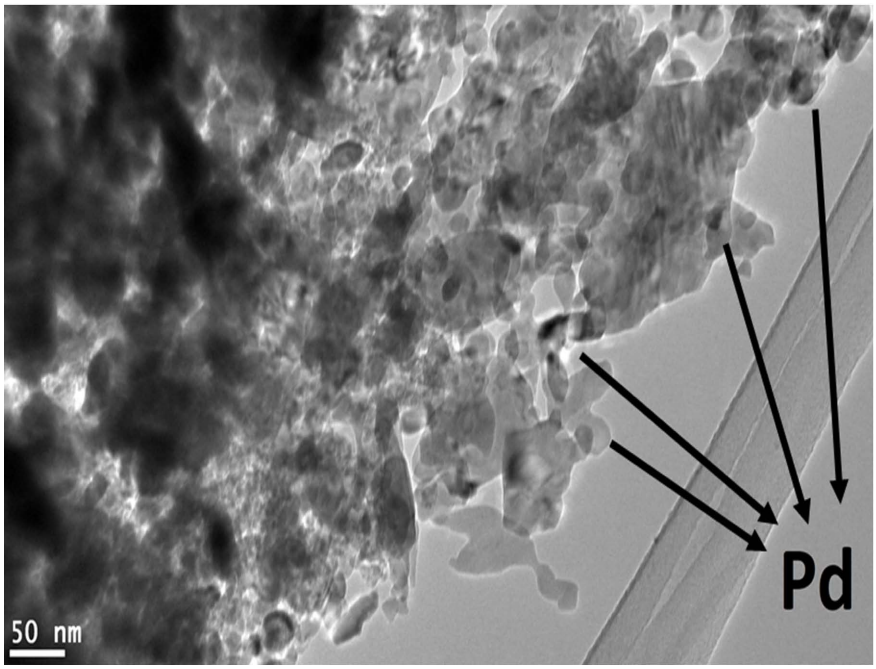

Figure 7. TEM images of ZnTiAl-Pd-LDO.

3.8. The Photocatalytic Performance for the Production of Hydrogen from Glucose

The photocatalytic reactions were performed in an inner irradiation system with a closed-equipped gas recirculation. A Pyrex cell with a flat window for illumination in all the experiments where photodeposition of palladium was loaded on the surface of layered double hydroxides (LDHs). Then, powder (1.0 wt%) of palladium chloride (II) ($PdCl_2$, Aldrich 99%) was added and dissolved in a solution of 10 ml deionized water. Then, 1 gram of LDHs was added to the mixture to obtain the palladium loading onto the surface of LDH. The photoreduction process was performed to highlight the comment period of 120 minutes with Xeon lamp light 400 W. It was dried in an oven at 40˚C for one night.

It is giving the product Pd/LDHs. Then, calcination of catalysis by air at a temperature of 400˚C for 4 h, then grounded, giving the product layered double oxide (Pd/LDO). About 0.080 mg of catalyst was used for the decomposition of the total liquid volume, which was around 40 mL of deionized water and (1.00 mg 0.0055

Mol) from glucose. The reaction system was evacuated by a mechanical pump and then filled with 1 MPa of high-purity N_2 (>99.99%). The hydrogen generation rate was obtained in a pure N_2 atmosphere. The hydrogen evolution initially increases with reaction time [21]. This process was repeated five times in order to remove O_2 from the system [22]. Powder photocatalysts were dispersed in the water by stirring with a magnetic stirrer. The temperature of the solution was controlled at about 40˚C by circulating water, and the reaction was conducted for 5 hours under 400 W Xe-lamp irradiation wavelength 365 nm. The 1.0 ml was taken from the bag gas sample. Periodically, during these experiments, a narrow gas syringe was injected into the analyzer SHIMADZU Gas Chromatograph (SGC). The detector was (DTCD1) type, and N_2 was used as a constant flow of carrier gas. The injector executor temperature was set at 90˚C, but the detector temperature column was set at 150˚C to detect the sample gas sample injected existing in the gas sample, which was replaced at the thermal conductivity of greenhouse gases to give quantitative and qualitative data for the gas sample.

4. Photocatalytic Activity

Photocatalytic performance shows the influence of the Pd-LDO concentration on hydrogen production from glucose during the UV irradiation time.

Effect of M^{2+}/TiAl-Pd-LDO (M = Mg, Ni, and Zn): In H_2 Production

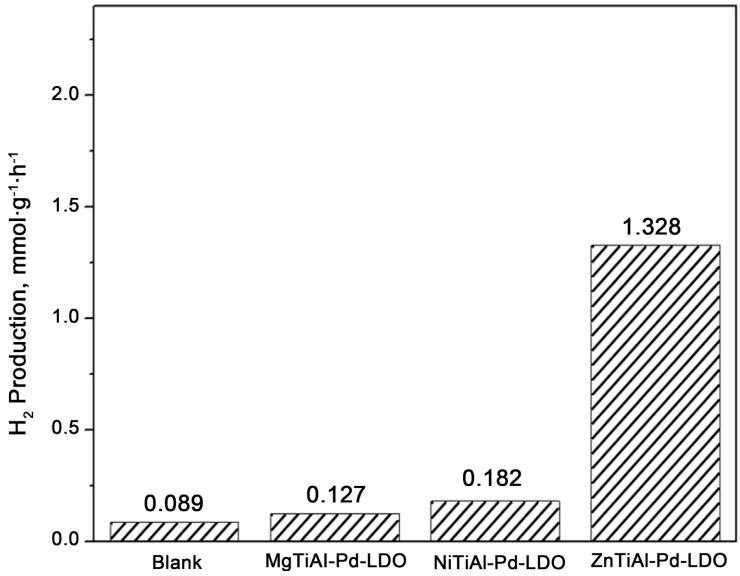

Figure 8. The amount of hydrogen determined after 5 h of photocatalytic reaction, 80 mg of catalyst, 1 g of glucose in 40 mL of deionized water by 400 W Xe-lamp UV 365 nm irradiation by using Pd 1.0 wt% on M^{2+}/TiAl-Pd-LDO (M = Mg, Ni and Zn).

Figure 8 shows the hydrogen production rate of different M^{2+}/TiAl-Pd-LDO (M^{2+} = Mg, Ni, and Zn) catalysts. It is observed by changing the type of metals. The hydrogen production rate is changing. In addition, we were trying to determine

the influence of activation energy on the difference in the hydrogen production rate for M^{2+}/TiAl-Pd-LDO (M^{2+} = Mg, Ni and Zn). This result displays remarkable photocatalytic performance for glucose in hydrogen production. It is noted that ZnTiAl-Pd-LDO has the best performance in hydrogen production from glucose with (1.328 mmol·g^{-1}·h^{-1}) of the amount of hydrogen as compared with NiTiAl-Pd-LDO (0.182 mmol·g^{-1}·h^{-1}) and MgTiAl-Pd-LDO (0.127 mmol·g^{-1}·h^{-1}). Hydrogen production gradually increases with the change of the metals. This indicates a lack of regularity of Ni and Mg with glucose in hydrogen production. Moreover, catalysts containing Zn metal have higher photoactivity than other metals. Band gap energy, which is calculated from the UV spectrum, also supports this result. It is reported that highly dispersed active metals that help to increase photocatalysis effective sites enhance the efficiency of electron separation holes.

5. Conclusion

The crystallographic data of the M^{2+}/TiAl-Pd-LDO (M = Mg, Ni and Zn) catalyst were effectively prepared by fluorescence deposition and hydrothermal film synthesis at high temperatures, which XRD, BET, ICP-AES, and UV-vis analysis confirmed. It is noted that ZnTiAl-Pd-LDO has the best performance and activity photocatalyst in hydrogen production from glucose with (1.328 mmol·g^{-1}·h^{-1}) of the amount of hydrogen as compared with NiTiAl-Pd-LDO (0.182 mmol·g^{-1}·h^{-1}) and MgTiAl-Pd-LDO (0.127 mmol·g^{-1}·h^{-1}). Catalyst ZnTiAl-Pd-LDO (204.2645 m^2/g) gives a large surface area for activity UV radiation among the other catalysts as compared with catalyst NiTiAl-Pd-LDO (175.5964 m^2/g) and catalyst MgTiAl-Pd-LDO (116.3723 m^2/g), due to their specific surface area domain preference and band gaps. This was the opposite of the result for the photocatalytic activity for these (ZnTiAl-Pd-LDO, NiTiAl-Pd-LDO, and MgTiAl-Pd-LDO). This work not only provided important and accurate insight into the construction rules of catalysts but also gave a clear understanding of the design and the synthesis of Zn-containing LDOs and related materials with prospective applications in photocatalysis in hydrogen production.

Acknowledgements

The authors would like to thank King Abdulaziz City for Science & Technology (KACST) for financially support this work.

Conflicts of Interest

The authors declare no conflicts of interest regarding the publication of this paper.

References

[1] Lu, J., Zahedi, A., Yang, C., Wang, M. and Peng, B. (2013) Building the Hydrogen Economy in China: Drivers, Resources and Technologies. *Renewable and Sustainable Energy Reviews*, **23**, 543-556. https://doi.org/10.1016/j.rser.2013.02.042

[2] Chaubey, R., *et al.* (2013) A Review on Development of Industrial Processes and

Emerging Techniques for Production of Hydrogen from Renewable and Sustainable Sources. *Renewable and Sustainable Energy Reviews*, **23**, 443-462.

[3] Fujishima, A. and Honda, K. (1972) Electrochemical Photolysis of Water at a Semiconductor Electrode. *Nature*, **238**, 37-38. https://doi.org/10.1038/238037a0

[4] Veziroğlu, T.N. and Şahin, S. (2008) 21st Century's Energy: Hydrogen Energy System. *Energy Conversion and Management*, **49**, 1820-1831. https://doi.org/10.1016/j.enconman.2007.08.015

[5] Al-Mazroai, L.S., Bowker, M., Davies, P., Dickinson, A., Greaves, J., James, D., *et al.* (2007) The Photocatalytic Reforming of Methanol. *Catalysis Today*, **122**, 46-50. https://doi.org/10.1016/j.cattod.2007.01.022

[6] Cargnello, M., Gasparotto, A., Gombac, V., Montini, T., Barreca, D. and Fornasiero, P. (2011) Photocatalytic H_2 and Added-Value By-Products—The Role of Metal Oxide Systems in Their Synthesis from Oxygenates. *European Journal of Inorganic Chemistry*, **2011**, 4309-4323. https://doi.org/10.1002/ejic.201100532

[7] Faria, J.L.F.J., Pereira, M.M. and Faria, J. (2008) Catalysis from Theory to Application: An Integrated Course: An Integrated Course. Imprensa da Universidade de Coimbra/Coimbra University Press, 477-494.

[8] Herrmann, J. (2005) Heterogeneous Photocatalysis: State of the Art and Present Applications in Honor of Pr. R.L. Burwell Jr. (1912-2003), Former Head of Ipatieff Laboratories, Northwestern University, Evanston (Ill). *Topics in Catalysis*, **34**, 49-65. https://doi.org/10.1007/s11244-005-3788-2

[9] Xia, S., Zhang, L., Zhou, X., Pan, G. and Ni, Z. (2015) The Photocatalytic Property for Water Splitting and the Structural Stability of CuMgM Layered Double Hydroxides (M = Al, Cr, Fe, Ce). *Applied Clay Science*, **114**, 577-585. https://doi.org/10.1016/j.clay.2015.06.023

[10] Gastuche, M.C., Brown, G. and Mortland, M.M. (1967) Mixed Magnesium-Aluminiun Hydroxides. I. Preparation and Characterization of Compounds Formed in Dialysed Systems. *Clay Minerals*, **7**, 177-192. https://doi.org/10.1180/claymin.1967.007.2.05

[11] Gusmano, G., Nunziante, P., Traversa, E. and Chiozzini, G. (1991) The Mechanism of $MgAl_2O_4$ Spinel Formation from the Thermal Decomposition of Coprecipitated Hydroxides. *Journal of the European Ceramic Society*, **7**, 31-39. https://doi.org/10.1016/0955-2219(91)90051-z

[12] Peng, S., Peng, Y., Li, Y., Lu, G. and Li, S. (2009) Photocatalytic Hydrogen Generation Using Glucose as Electron Donor over Pt/$Cd_XZn_{1-x}S$ Solid Solutions. *Research on Chemical Intermediates*, **35**, 739-749. https://doi.org/10.1007/s11164-009-0091-z

[13] Kawai, M., Kawai, T. and Tamaru, K. (1981) Production of Hydrogen and Hydrocarbon from Cellulose and Water. *Chemistry Letters*, **10**, 1185-1188. https://doi.org/10.1246/cl.1981.1185

[14] Deák, Á., Janovák, L., Csapó, E., Ungor, D., Pálinkó, I., Puskás, S., *et al.* (2016) Layered Double Oxide (LDO) Particle Containing Photoreactive Hybrid Layers with Tunable Superhydrophobic and Photocatalytic Properties. *Applied Surface Science*, **389**, 294-302. https://doi.org/10.1016/j.apsusc.2016.07.127

[15] Lu, L., Wu, Z., Bi, J., Zhang, H. and Shahab, A. (2024) Calcined MgFe Layered Double Hydroxides for Magnetic Separation and Enhanced Adsorption Performance of Methyl Orange: Mechanism Based on the Memory Effect. *Journal of Water Process Engineering*, **63**, Article ID: 105418. https://doi.org/10.1016/j.jwpe.2024.105418

[16] Pinnavaia, T.J. (1983) Intercalated Clay Catalysts. *Science*, **220**, 365-371.

https://doi.org/10.1126/science.220.4595.365

[17] Centi, G. and Perathoner, S. (2008) Catalysis by Layered Materials: A Review. *Microporous and Mesoporous Materials*, **107**, 3-15. https://doi.org/10.1016/j.micromeso.2007.03.011

[18] Cavani, F., Trifirò, F. and Vaccari, A. (1991) Hydrotalcite-Type Anionic Clays: Preparation, Properties and Applications. *Catalysis Today*, **11**, 173-301. https://doi.org/10.1016/0920-5861(91)80068-k

[19] Gaines, R.V., *et al.* (1997) Dana's New Mineralogy: The System of Mineralogy of James Dwight Dana and Edward Salisbury Dana. Wiley, 1011 p.

[20] Zhu, Y., Laipan, M., Zhu, R., Xu, T., Liu, J., Zhu, J., *et al.* (2017) Enhanced Photocatalytic Activity of Zn/Ti-LDH via Hybridizing with C60. *Molecular Catalysis*, **427**, 54-61. https://doi.org/10.1016/j.molcata.2016.11.031

[21] Zhao, Y., Chen, P., Zhang, B., Su, D.S., Zhang, S., Tian, L., *et al.* (2012) Highly Dispersed TiO_6 Units in a Layered Double Hydroxide for Water Splitting. *Chemistry—A European Journal*, **18**, 11949-11958. https://doi.org/10.1002/chem.201201065

[22] Amin, M.T., Alazba, A.A. and Shafiq, M. (2021) Synthesis and Characterization of Zn/Fe Layered Double Hydroxide and Its Composites for Copper Adsorption from Aqueous Solution. *Desalination and Water Treatment*, **218**, 281-293. https://doi.org/10.5004/dwt.2021.26948

[23] Zhao, Y., Chen, P., Zhang, B., Su, D.S., Zhang, S., Tian, L., *et al.* (2012) Highly Dispersed Tio_6 Units in a Layered Double Hydroxide for Water Splitting. *Chemistry—A European Journal*, **18**, 11949-11958. https://doi.org/10.1002/chem.201201065

[24] Vaiano, V., Iervolino, G., Sarno, G., Sannino, D., Rizzo, L., Murcia Mesa, J.J., *et al.* (2015) Simultaneous Production of $Ch_4$and H_2 from Photocatalytic Reforming of Glucose Aqueous Solution on Sulfated Pd-TiO_2 Catalysts. *Oil & Gas Science and Technology*, **70**, 891-902. https://doi.org/10.2516/ogst/2014062